ACS MATERIALS LETTERS

Letter

Observations of 3 nm silk nanofibrils exfoliated from natural silkworm silk fibers

Qi Wang, Shengjie Ling, Quanzhou Yao, Qunyang Li, Debo Hu, Qing Dai, David A. Weitz, David L Kaplan, Markus J. Buehler, and Yingying Zhang

ACS Materials Lett., **Just Accepted Manuscript** • DOI: 10.1021/acsmaterialslett.9b00461 • Publication Date (Web): 03 Jan 2020

is published by the American Chemical Society. 1155 Sixteenth Street N.W., Washington, DC 20036

Observations of 3 nm silk nanofibrils exfoliated from natural silkworm silk fibers

Qi Wang[1,5†], Shengjie Ling[2,6,7†], Quanzhou Yao[3], Qunyang Li[3], Debo Hu[4], Qing Dai[4], David A. Weitz[5], David L. Kaplan[6*], Markus J. Buehler[7*], Yingying Zhang[1*]

[1] Key Laboratory of Organic Optoelectronics and Molecular Engineering of the Ministry of Education, Department of Chemistry, Tsinghua University, Beijing 100084, China

[2]School of Physical Science and Technology, ShanghaiTech University, Shanghai 201800, China

[3]Center for Nano and Micro Mechanics, Applied Mechanics Laboratory, Department of Engineering Mechanics, School of Aerospace, Tsinghua University, Beijing 100084, China

[4]Nanophotonics Research Division, CAS Center for Excellence in Nanoscience, National Center for Nanoscience and Technology, Beijing 100190, China

[5]School of Engineering and Applied Sciences, Harvard University, Cambridge, MA 02138, USA

[6]Department of Biomedical Engineering, Tufts University, Medford, MA, 02155, USA

[7]Department of Civil and Environmental Engineering, Massachusetts Institute of Technology, Cambridge, MA, 02139, USA

†These authors contributed equally to this work.

Correspondence to
yingyingzhang@tsinghua.edu.cn; david.kaplan@tufts.edu; and mbuehler@mit.edu

ABSTRACT: Silk fibers are one of the most attractive natural materials which exhibit enchanting lustre and superior mechanical properties. Exploring the unique hierarchical architecture structures of natural silk fibers is the basis to understand these unique properties. Here we report observations of 3.1±0.8 nm silk nanofibrils and 3.7±0.9 Å silk molecule chains exfoliated from natural silkworm silk fibers. Interestingly, the individual nanofibrils and protein chains show periodic diameters fluctuating along their axes. We further find the thicker regions are relatively softer and the thinner regions stiffer, and these can be assigned to alternatively distributed α-helix and β-sheet domains,

respectively. Based on these observations, we proposed a refined structure model of natural silk, which ranges from the molecular level to the fiber scale. These findings provide new opportunities to understand and exploit the unique structure-property relationships found in natural silk fibers, including inspiring the design of new artificial materials.

Nature has its own secrets in the design of material structures to achieve the required performance. Many natural materials, such as silk, wood and mollusc shells, show superior mechanical properties even though their components consist of relatively simple components or building blocks.[1-5] The secret to these structures lies in their hierarchical assembly, spanning angstrom to macroscopic levels, starting from the basic building blocks.[6-8] Therefore, scientists continue to explore these structures to understand the origins of the unique mechanical properties of the nature materials, while also looking for inspiration in the design of artificial materials. Silk is a well-known natural protein fiber which exhibits superior mechanical properties including high tensile strength (0.3-1.3 GPa) and high elongation at break (4-38%).[9-11] These mechanical features enable natural silk fibers to absorb tremendous energy before breaking, resulting in extraordinary toughness (70-200 MJ m^{-3}) that is higher than steel (6 MJ m^{-3}) or Kevlar fibers (50 MJ m^{-3}).[8, 12-14] Many studies have reported the fabrication of artificial silk fibers using regenerated silks.[15-17] However, the mechanical properties of such artificial silk fibers remain inferior to the natural counterparts although the main components are the same. Therefore, it is important to investigate the sophisticated hierarchical structure of natural silk fibers to further understand the origins of these properties.

Early work was carried out to investigate the structure of natural silk fibers.[8, 12, 18-22] For instance, Miller et al.[20] reported that the observation of nanofibrils with diameters of ~59 nm extending parallel to the fiber axis using atomic force microscopy (AFM) and small angle X-ray scattering (SAXS) from freshly exposed internal surfaces by peeling silk fibers. Similar results were reported by Liu et al.[8, 12, 21] and Putthanarat et al.[22], showing that silk fibers consisted of a bundle of silk fibrils, with diameters of the fibrils around 20-100 nm. The secondary structural analysis by X-ray diffraction and ^{2}H solid state nuclear magnetic resonance (NMR) indicated that β-sheet crystallites in these natural silk fibers were predominantly aligned with the fiber axis.[23-24]

Based on these experimental results, structural models, such as the two-phase cross-linking network model,[25] mean field theory based order/disorder fraction model[26-27] and Maxwell model,[28-29] were proposed to interpret the mechanical properties of silks. For example, two-phase cross-linking network model regards silk fibers as a rubber-like network structure, in which β-sheets serve as crosslinkers to connect the amorphous regions together.[25] Mean field theory based order/disorder fraction model simplifies the silk fibroin molecular chain to polyalanine chain and transfer the condensed state structure of silk fiber into ordered/unordered fraction.[26-27] Maxwell model treats the β-sheet nanocrystals and amorphous structures as purely elastic springs and viscous dampers.[28-29] In these models, silk fibers were simplified into uniform semicrystalline polymer-like fibers with highly-oriented antiparallel β-sheet nanocrystals embedded in the amorphous matrix (consisting of random coil and/or helix structures).[30] As a result, these models can predict the mechanical behavior of silk fibers as also found in other polymers, such as thermo-mechanical properties and viscoelasticity.

However, those models cannot interpret the unique mechanical behavior of silk fibers that are not found in common polymer materials. For example, defects usually are seeds for polymer materials failure due to the localized stress concentrations. However, defects in silk fibers (*e.g.*, cavities, cracks, tears), which can reach several hundred nanometers in size, have no significant impact on the mechanical response of the fibers.[31] In addition, silk fibers exhibit ductile failure even at ultralow temperatures (-196°C).[32] In contrast, polymer materials that are flexible at room temperature, such as nitrile rubber, lose elasticity or break during immersing in liquid nitrogen due to polymer chain segments are frozen when the environmental temperature lower than its glass transition temperature. The lack of deeper experimental observations into the hierarchical structures in natural silk fibers prevents further insights into the underlying structure-property dependence of silk fibers.

The most significant obstacle to experimentally examine the structure of silk fibers at multiscale levels, especially at the nanoscale and sub-nanoscale, is the lack of an effective approach to controllably reverse engineer silk fibers while keeping the structure of the building blocks at each level undamaged. Binary-solvents, such as LiBr/H_2O[33] and $CaCl_2$/formic acid[34], are established as extraction solvents for silk fibers, but dissolve the silk fibers into silk fibroin molecules with unwanted degradation. In addition to chemical exfoliation approaches, peeling process have been developed,[20-22] which can expose the inner structures of silk fibers. This approach provides opportunities to see the rough surface of the randomly exposed fiber sections and some nano-fibrils (20-100 nm) on the surface. However, the 3D structures of the nano-fibrils and the sophisticated architectures below 20-100 nm remain unknown.

Herein, we report a new top-down strategy to gradually exfoliate silkworm silk fibers into their basic building blocks, only breaking the hydrogen bonds within the aligned nanofibrils and the polypeptide chains. Individual silk nanofibrils (SNFs) with diameters down to 3.1±0.8 nm, and even silk molecule chains with diameters of 3.7±0.9 Å, which retained their pristine structures, were successfully obtained. In addition, the secondary structure organization of silk fibroin protein in these nanofibrils was investigated using force-modulation AFM (FM-AFM) and Fourier-transform infrared spectroscopy (FTIR). The experimental results reveal the basic building blocks of natural silk fibers and their assembled structures. Based on the characterization, we propose a refined structural model of natural silkworm silk fibers regarding their hierarchical structures. Understanding the hierarchical architectures in silk fibers offers fundamental insight into natural structure design strategies and also inspires the design and construction of high-performance artificial materials.

Figure 1a illustrates the hierarchical exfoliation of *B. mori* silkworm cocoon silk fiber and **Figure 1b** shows the raw silk fiber. First, the outside layer of silk fibers, consisting of sericin and glycoprotein, was removed by boiling in 0.5% (w/w) Na_2CO_3 solution for 30 min. The degummed silk fibers were washed thoroughly with distilled water and allowed to air dry at room temperature.[35] Scanning electron microscopy (SEM) examination confirmed the thorough removal of the residues. The resultant silk fibroin filaments present typical triangular cross-sections with a diameter of ~10 μm (**Figure 1c**). Recently, we found that hexafluoroisopropanol (HFIP), a well-known hydrogen-bond-breaking denaturant,[36] can partially dissolve *B. mori* silkworm cocoon silk fibers to microfibrils with diameters of 5-50 μm and contour lengths of 50-500 μm after incubating silk fiber/HFIP (at a weight ratio, 1:30) mixtures at 60°C.[37] Herein, we reasoned that silk fibers could be gradually exfoliated into nanostructures and even molecular scale proteins using the same dissolution process but a longer incubation time. A modified HFIP-based procedure was applied to exfoliate the hierarchical structures of the silk fibroin filaments (see Methods for details). During the incubation process, the gradual transition of silk fiber/HFIP solution from opaque to transparent with increasing incubation time within 48 h implied that the visible microscale fibers were dissociated into smaller structures with dimensions smaller than the visible wavelength (**Figure S1**). High-resolution SEM images (**Figure 1d and Figure S2**) disclosed silk filaments directly exfoliated into fibrils with diameters of 20-100 nm and lengths up to several microns. Interestingly, we observed periodic height fluctuation along the contour of the fibrils with pitches of 75-100 nm, which are proposed to correspond to helical structures similar to those found in amyloid fibrils,[38] but not previously observed in silk fibers.

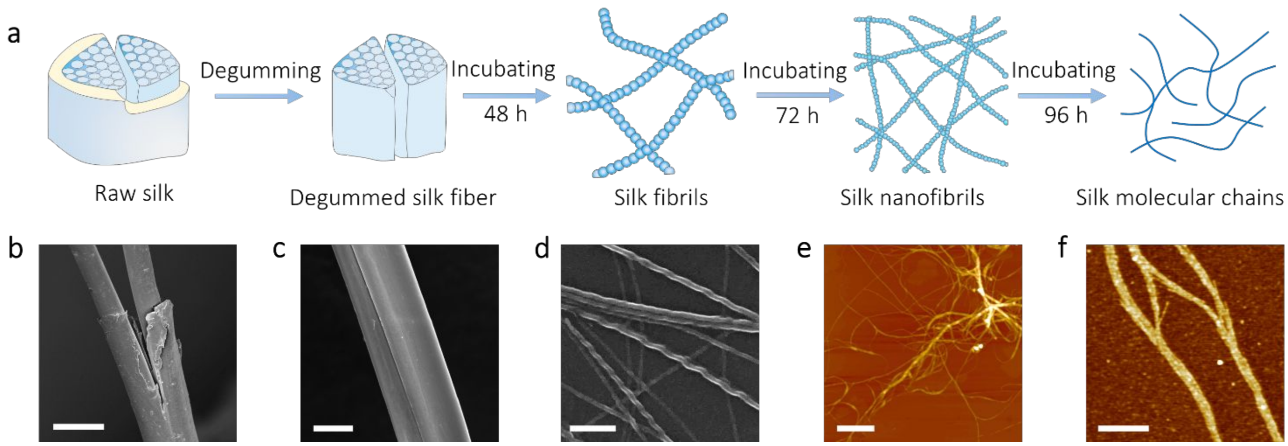

Figure 1. Exfoliation process for silk fibers and images of silk fibers/fibrils that range from micro to subnano scales. a, Schematic of the process to exfoliate silk fibers from raw silk fiber into silk molecular chains. **b-d**, SEM images of raw silk fiber, degummed silk fiber and silk fibrils. **e-f**, AFM images of silk nanofibrils and silk molecular chains. Scale bars, 10 μm (b), 5 μm (c), 200 nm (d), and 2 μm (e), 500 nm (f).

For further exfoliation, we extended the incubation time from 48 h to 72 h and found the silk fibrils were further split into nanofibrils with diameters of 2-4 nanometers (**Figure 1e and Figure S3**). **Figure 1e** shows that a thicker fibril was composed of a bundle of parallel aligned nanofibrils. When we further extended the incubation time to 96 h, some fibrous aggregates (**Figure 1f**) with diameters of only several angstroms were observed. The dimensions of the sub-nanometer fibrils were several times smaller than that of protein secondary structures, *i.e.*, β-sheet, random coil and/or helix. The size was closer to that of amino acids.[39] Based on these observations, we propose that these aggregates are the assembly of single silk fibroin molecular chains. Previously, only globular structures of silk fibroin chains with sizes of 20-100 nm were observed using AFM and SEM.[19-20, 40] As has been verified by various characterization methods, the nanocrystalline regions in natural silk fibers are partially oriented along the axis of the fiber. [41-42] This oriented nanocrystal structures play essential roles in the high strength of silk fibers.

With the aim of insight into the structural details of these nanofibrils and molecular chains in silk fibers, high-resolution AFM was accessed to image these structures. In these experiments, we focused on analyzing the height of the structures rather than the width, since the width information extracted from AFM measurements can be affected by the shape and radius of the AFM tip. The topological structures of single silk nanofibrils are given in **Figure 2a-c and Figure S4**. The diameter of these nanofibrils was around ~3 nm with the length reaching 10 μm. The partially exfoliated silk fibrils were a few times higher than the typical 3-nm silk nanofibrils. The longitudinal height profile along the blue trace in **Figure 2a** demonstrates the periodic diameter fluctuation of the nanofibrils with a periodicity of ~0.24 μm (the blue line in **Figure 2b**). After performing statistical analysis on the diameter of single nanofibrils (100 individual nanofibrils and 930 data points), we found the diameter distribution fit well with a Gaussian distribution with a center value of 3.1 ± 0.8 nm (**Figure 2c**). This feature indicates that the diameter of the natural silk nanofibrils is around 2-4 nm, which agrees well with the average height of the silk nanofibrils (2-4 nm) formed from silk fibroin aqueous solution in bottom-up methods.[43] Previous experiments proved that AFM images are the result of a convolution of the imaging-tip's shape with the object's actual shape, so the width of silk nanofibrils can not be measured by AFM.[44-45] Our previous simulation results disclosed that the nano-confined scale of β-sheets makes the most efficient use of hydrogen bonds and leads to the emergence of dissipative molecular stick-slip deformation, achieving higher strength, stiffness, and toughness than that found in larger nanocrystals.[18] The diameter of the obtained silk nanofibrils fit well with the size of nano-crystalline β-sheets.

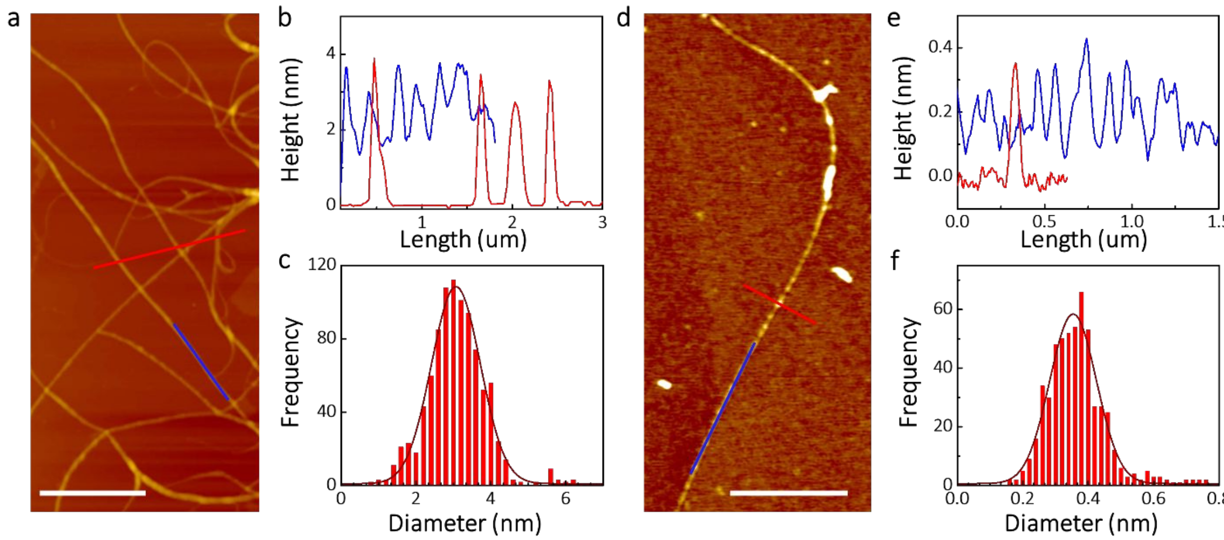

Figure 2. Topological AFM images, profiles and the distribution of silk nanofibril and silk molecular chain diameters. a, Topgraphic image of silk nanofibrils. Scale bar, 2 μm. **b**, Longitudinal (blue curve) and transversal (red curve) height profiles of the silk nanofibrils as indicated in (a). **c**, Histogram and Gaussian fit showing the diameter of nanofibrils around 3.0 nm. **d**, Topgraphic image of silk molecular chain. Scale bar, 1 μm. **e**, Longitudinal (blue curve) and transverse (red curve) height profiles of the silk molecular chain as indicated in **d**. **f**, Histogram and Gaussian fit of silk molecular chains showing the diameter of molecuar chains around 3.7 Å.

We also characterized the structures of single silk fibroin molecular chain exfoliated from the ~3 nm nanofibrils. Some typical AFM images of these chains are shown in **Figure 2d and Figure S5**. The statistical diameter of the silk fibroin molecular chains was 3.7 ± 0.9 Å (**Figure 2f**), corresponding to the dimensions of the repetitive sequence of the heavy chain of *B. mori* silkworm silk fibroin (GAGAGS and GAGAGY).[14] However, the length of the molecular chain (more than 4 μm) was larger than the length calculated from the average molecular weight of silk fibroin. This difference might be ascribed to the complex compositions of silk fibroin and the potential chelating effects of chain termini between two chains. The silk fibroin molecule chains also showed a periodical necklace-like morphology with a period of ~0.1 μm (the blue line in **Figure 2e**), similar to the observed fluctuation in diameter of the silk nanofibrils.

In order to investigate the protein conformation in individual silk nanofibrils, particularly the distribution of the tightly packed β-sheets and poorly orientated α-helix,[46-47] FM-AFM was used to simultaneously obtain topography images and relative stiffness maps.[48-49] **Figure 3 a-e** show the topography and corresponding relative stiffness contrast mapping of silk nanofibrils deposited on mica. **Figure 3f** shows the topography on a polydimethylsiloxane (PDMS) substrate. Both the two topography images show periodic variation in the height of the fibril along the axis direction. Similar to the periodic height of individual silk nanofibrils, the relative stiffness also displayed a periodic distribution (**Figure 3c, Figure 3e and Figure 3g**). The higher regions in the images along the single nanofibrils were relatively softer and the lower regions were relatively stiffer. These results can be attributed to protein heterogeneity in secondary structure. The stiffer regions can be assigned to β-sheets and the relative soft parts can be assigned to α-helices. Thus, the thicker and thinner regions along the silk nanofibrils are mainly composed of α-helices and β-sheets, respectively.

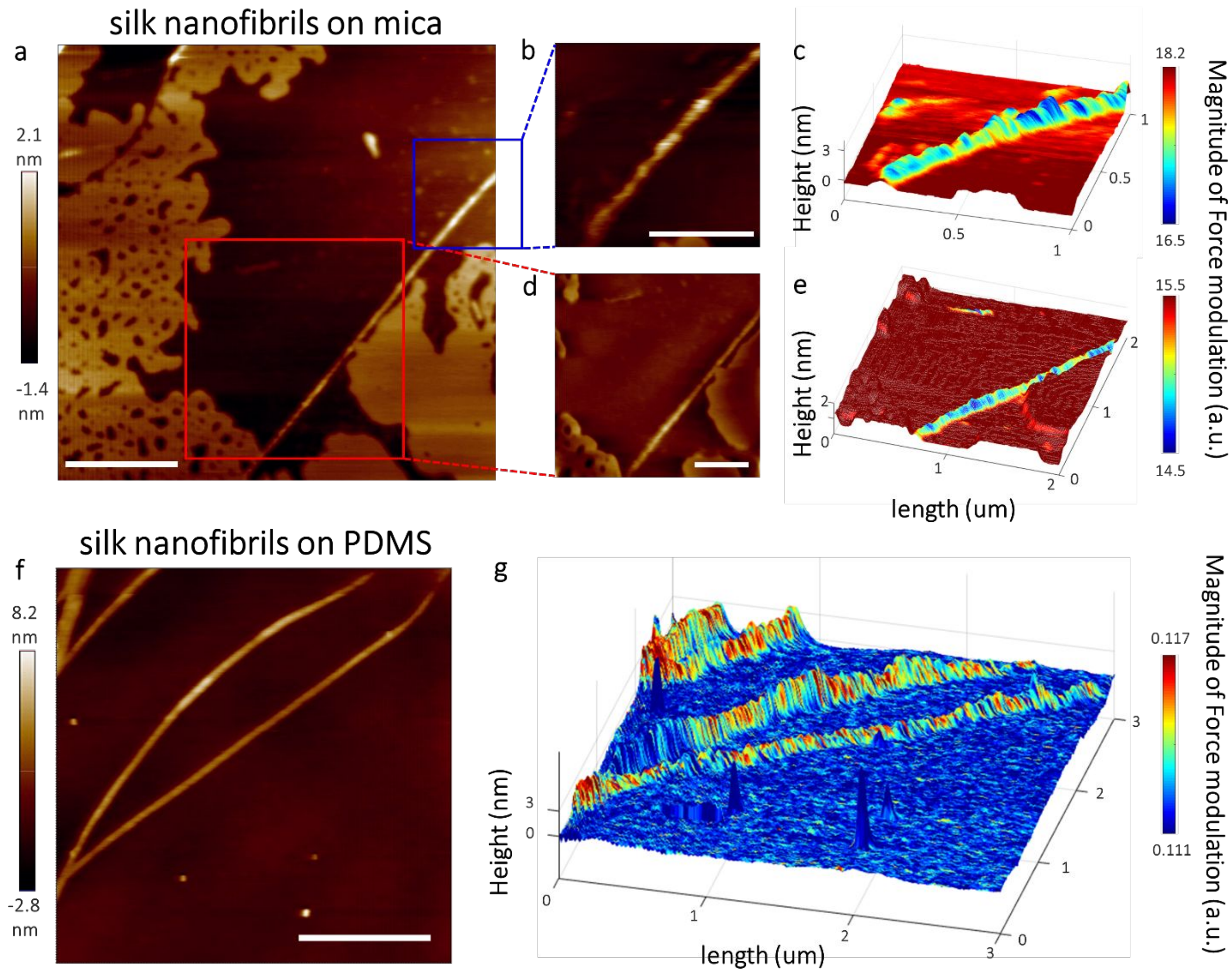

Figure 3. FM-AFM images of silk nanofibrils deposited on mica and PDMS showing acqured topography and relative stiffness mapping. a, Topgraphic image of silk nanofibrils on mica. Scale bar, 1 μm. **b,d**, AFM images of silk nanofibril in (**a**). Scale bars, 0.5μm. **c,e**, Relative stiffness mapping of silk nanofibrils using force-modulation mode of AFM corresponds to (b) and (d), respectively. **f**, Topography of SNFs on PDMS. Scale bar, 1 μm. **g**, Relative stiffness mapping of SNFs using force-modulation mode of AFM corresponds to (f). To exclude the effect of the substrate, nanoscale relative stiffnes mapping of SNFs deposited on PDMS also conducted. Different from mica substrate, SNFs is relatively stiffer compared with PDMS.

Futhermore, we also compared the secondary structures of silk nanofibrils and silk fibers by FTIR spectra (**Figure 4**). Standard deconvolution of amide I band of silk nanofibrils dispersed in water and HFIP showed similar shapes to degummed silk fibers. Three major peaks in 1639, 1670, and 1697 cm^{-1} were assigned to β-sheet, α-helix, and β-turn, respectively. Quantitative analysis reveals that silk nanofibrils and silk fibers are consist of 40-42% β-sheet crystallites, confirming that silk nanofibrils and natural silk fibers shared the similar secondary structures.

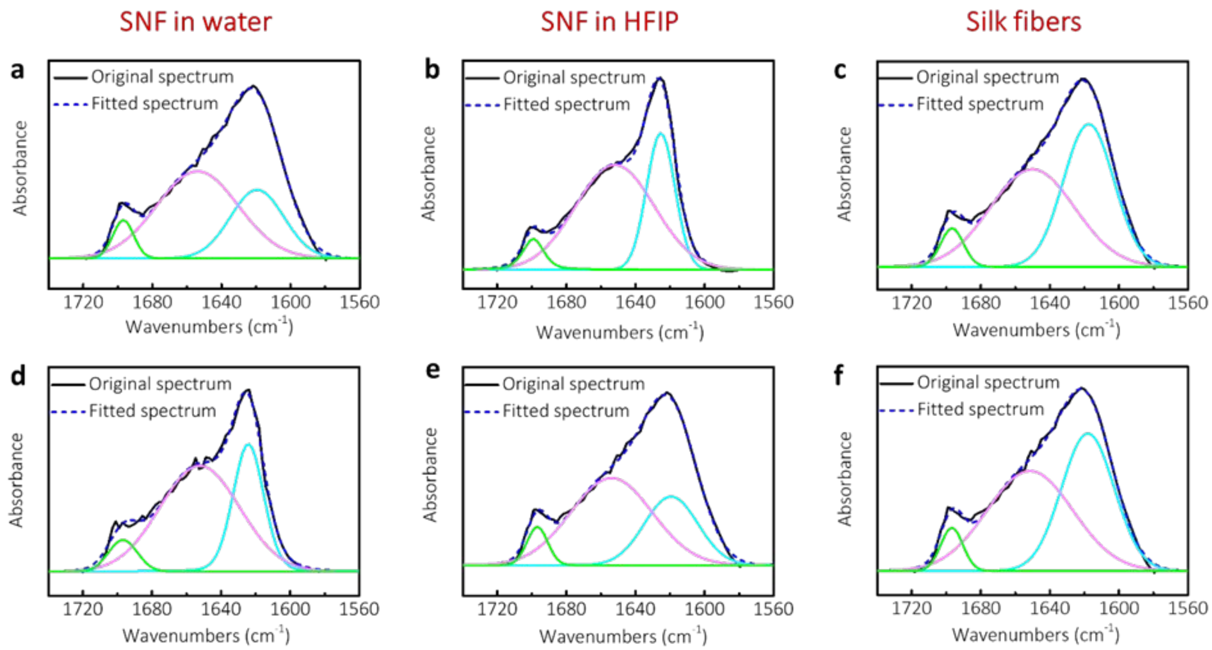

Figure 4. Deconvolution of FTIR spectra in amide I band of SNFs and silk fibers. First column spectra (a,d) correspond to SNFs despersed in water. Second column spectra (b,e) correspond to SNFs despersed in HFIP. Third column spectra (c,f) correspond to degummed silk fibers. The plots show the original spectra (black solid line), the fitting line (blue dotted line), and their deconvoluted traces (three smooth Gaussian curves).

Based on the above experimental observations and previously reports,[47, 50] we proposed a refined hierarchical structural model of natural *B. mori* silkworm silk fiber (**Figure 5**). At the molecular scale, it is composed of highly repetitive amino acid sequences, alternating between hydrophilic (GAGAGY) and hydrophobic (GAGAGS) segments, and flanked by the highly conserved shorter terminal domains (N- and C-termini). During natural spinning, the hydrophilic regions maintain random coil and/or form into helical structures, while the hydrophobic domains transform into highly ordered β-sheet structures through extrusion and shear flow. These amorphous (random coil and/or helical) and nanocrystal (β-sheet) components are organized into silk nanofibrils with a diameter of ~3 nm, and then bundled into fibrils with diameters in the range of 20-100 nm, which are further assembled into silk fibroin fibers with a diameter of ~10 μm. This model contains two newly refined parts: (i) The β-sheet and random coil structures are arranged alternately in a single nanofibril, and there are mainly weak interactions (hydrogen bonds) rather than tangled molecular chains between neighboring silk nanofibrils. In contrast, the β-sheets served as cross-linkers to connect the neighboring nanofibrils in previous models.[22, 25, 51] (ii) The globular topological structure (globular protrusions) exists in three hierarchical levels, that is, molecular chain, nanofibril, and fibril, which contribute to the superior mechanical strength of silk fibers. When a silk fiber is subjected to tensile strain, the shear interlock between globules can increase shear stress transfer and lead to excellent resilience by 'shear locking', which was only demonstrated by previous molecular dynamics-based computational models.[50] Additional globules allows the tuning of free volume to adapt to wettability and against defects in silk fibers.

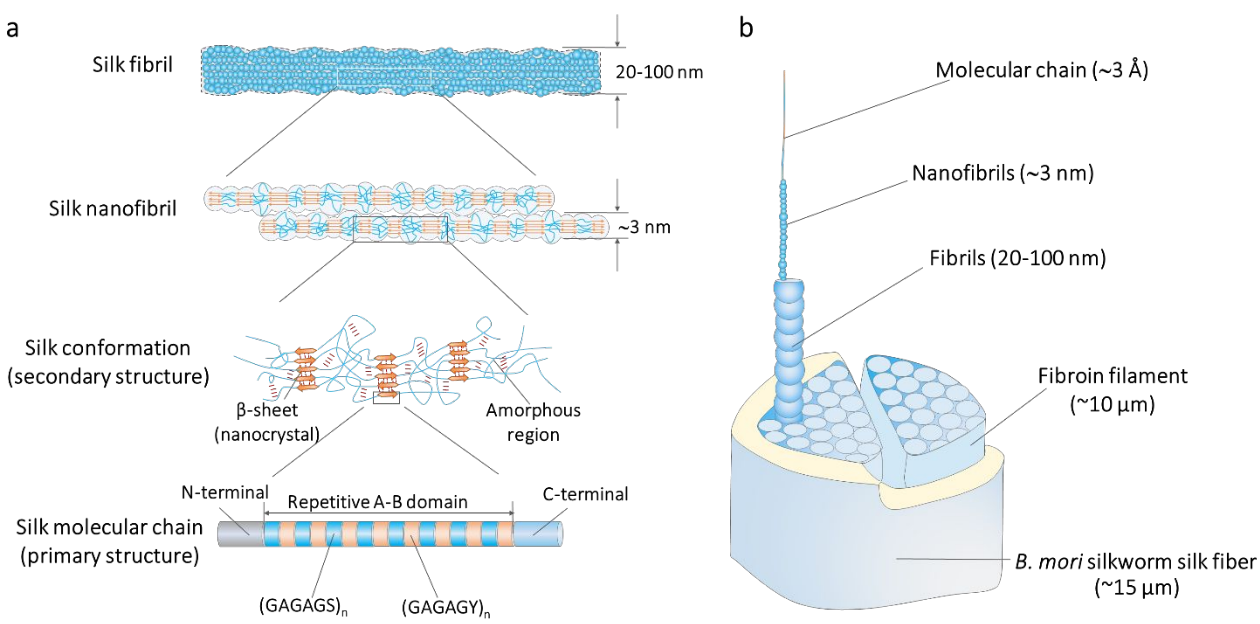

Figure 5. The proposed hierarchical structure of natural silkworm silk fiber. a, The silk molecular chain is composed of highly repetitive amino acid sequences (GAGAGS and GAGAGY). The random coil and/or helical structures and nanocrystal β-sheet components are organized into silk nanofibrils with a diameter of ~3 nm, which are bundled into fibrils with

diameters in a range of 20-100 nm. **b**, Illustration showing the hierarchical structre of silkworm silk fiber.

In summary, we investigated the sophisticated hierarchical structures of natural silk fibers by utilizing a step-by-step exfoliation process with natural silk fibers. By incubating silk fibers in HFIP, individual silk nanofibrils with diameters down to 3.1±0.8 nm and even silk molecule chains with diameters of 3.7±0.9 Å, which retained their pristine conformations, were selectively obtained by controlling the duration of incubation. This is the first report of extracting nanofibrils at the sub-nanometer scale from silk fibers. Intriguingly, both the ~3 nm nanofibers and the ~3.7 Å nanofibrils showed periodic fluctuations in diameters. We studied the morphology and the relative stiffness of individual silk nanofibrils using FM-AFM and found that the heterogeneity of secondary structures was consistent with the periodic variation in diameter of the individual silk nanofibrils. Based on the experimental findings, we proposed a refined hierarchical structure model of natural silks, ranging from the molecular level to the fiber scale. According to this refined model, the β-sheets and random coil structures are arranged alternately in a single nanofibril and these nanofibrils are parallelly aligned and form bundles in the natural silk fibers. The globular topological structure contributes to the superior mechanical strength of natural silk fibers. The findings in this work provide new opportunities to understand the structure-property relationships of natural silks, while also providing inspiration to the design and construction of superior engineering materials.

Liquid exfoliation of silk fibers. *B. mori* silkworm cocoons were cut into pieces and boiled in 0.02 M Na_2CO_3 for 30 min, then rinsed thoroughly with Milli-Q water for three times and allowed to air dry at room temperature. Then, the degummed silk fibers were immersed in pure HFIP

(Sigma-Aldrich, USA) with a weight ratio of 1:100 and then the airtight silk fiber/HFIP solution was incubated at 60°C without any destabilization. Previously, we used HFIP/filament mixtures with weight ratios of 30:1 or 20:1 to isolate the microfibrils.[52-53] In order to improve the exfoliation efficiency of HFIP, we increased the weight ratio to 100:1 and extended the incubation time to 48 h, while the temperature was still maintained at 60°C to avoid the evaporation of HFIP. Because the HFIP is a toxic solvent, all of these steps should be conducted in a chemical hood with the necessary precautions. The container used for liquid exfoliation must be tightly sealed to avoid evaporation of HFIP. With the increase of incubation time from 48 h to 108 h, the silk fibers were gradually exfoliated into silk fibrils, silk nanofibrils, and silk molecular chains. After incubation for the desired time, the containers were transferred to a chemical hood and used for preparing test samples.

Characterization. In order to characterize the dispersed individual nanofibril/molecular chain more clearly and conveniently, the silk/HFIP solution was diluted with Milli-Q water to a desired concentration of silk (100-200 μg/ml). 5 μl solution was deposited on a freshly cleaved mica surface for AFM characterization. Then, the sample was incubated for 10 min and dried under a stream of compressed air. All of these operations were carried out in the chemical hood. The morphologies of silk nanofibrils or silk molecular chains were characterized using a Cypher AFM (Oxford Instruments Asylum Research, Inc.). AFM imaging was performed by standard procedures in tapping mode at a scan rate of 1 Hz. AFM images were captured, flattened, and analyzed with Asylum Research software. SEM characterization was carried out using a Zeiss Ultra Plus filed emission scanning microscope (Carl Zeiss AG, Harvard University Center for Nanoscale Systems) operated at an acceleration voltage of 10 kV. To mitigate electrical charging effects, a 2-nm-thick Pd/Pt conductive layer was deposited on the surface using an EMS 300T D

Dual Head Sputter Coater. FTIR measurements were carried out using a Nicolet 6800 FTIR spectrometer with a diamond attenuated total reflectance accessory. For each measurement, 64 interferograms were co-added with a resolution of 4 cm^{-1}. Three kinds of samples, including silk nanofibrils dispersed in water, silk nanofibril dispersed in HFIP and silk fibers, were prepared on silicon wafers. The force-modulation atomic force microscopy characterizations were carried with an NtegraEx AFM (NT-MDT Spectrum Instruments, Inc.). The force modulation mode was performed with a rectangular silicon tip (cantilever B of CSC37, spring constant 0.3 N/m; conical shape tip with typical radius of 10 nm) at a frequency of 75 kHz and a driving amplitude of 1 mV. All of the characterization was carried out in air (RH ~25%) at room temperature.

Supporting Information.

Supplemental Information includes 5 figures.

Corresponding Author.

E-mail: yingyingzhang@tsinghua.edu.cn

ACKNOWLEDGMENTS

We thank Jingjie Yeo for many fruitful discussions and the assistance in computational simulations. We acknowledge the Harvard University Center for Nanoscale Systems (CNS) for providing part of the AFM and SEM measurements in this study. We thank the support of the National Natural Science Foundation of China (21975141,51672153) the National Key Basic Research and Development Program (2016YFA0200103) and the National Program for Support of Top-notch Young Professionals. We also thank the NIH (U01EB014976) for support for the study.

REFERENCES AND NOTES

(1) Song, J.; Chen, C.; Zhu, S.; Zhu, M.; Dai, J.; Ray, U.; Li, Y.; Kuang, Y.; Li, Y.; Quispe, N. Processing bulk natural wood into a high-performance structural material. *Nature* **2018,** *554*, 224.
(2) Mao, L.-B.; Gao, H.-L.; Yao, H.-B.; Liu, L.; Cölfen, H.; Liu, G.; Chen, S.-M.; Li, S.-K.; Yan, Y.-X.; Liu, Y.-Y. Synthetic nacre by predesigned matrix-directed mineralization. *Science* **2016,** *354*, 107-110.
(3) Tang, Z.; Kotov, N. A.; Magonov, S.; Ozturk, B. Nanostructured artificial nacre. *Nat Mater* **2003,** *2*, 413-8.
(4) Meyers, M. A.; Chen, P.-Y.; Lin, A. Y.-M.; Seki, Y. Biological materials: Structure and mechanical properties. *Prog Mater Sci* **2008,** *53*, 1-206.
(5) Wegst, U. G.; Bai, H.; Saiz, E.; Tomsia, A. P.; Ritchie, R. O. Bioinspired structural materials. *Nat Mater* **2015,** *14*, 23-36.
(6) Ling, S.; Kaplan, D. L.; Buehler, M. J. Nanofibrils in nature and materials engineering. *Nature Reviews Materials* **2018,** *3*, 18016.
(7) Nguyen, A. T.; Huang, Q. L.; Yang, Z.; Lin, N.; Xu, G.; Liu, X. Y. Crystal networks in silk fibrous materials: from hierarchical structure to ultra performance. *Small* **2015,** *11*, 1039-54.
(8) Du, N.; Liu, X. Y.; Narayanan, J.; Li, L.; Lim, M. L.; Li, D. Design of superior spider silk: from nanostructure to mechanical properties. *Biophys J* **2006,** *91*, 4528-35.
(9) Vollrath, F.; Knight, D. P. Liquid crystalline spinning of spider silk. *Nature* **2001,** *410*, 541-548.
(10) Vollrath, F.; Holtet, T.; Thogersen, H. C.; Frische, S. Structural organization of spider silk. *Proceedings of the Royal Society of London B: Biological Sciences* **1996,** *263*, 147-151.
(11) Yarger, J. L.; Cherry, B. R.; van der Vaart, A. Uncovering the structure–function relationship in spider silk. *Nature Reviews Materials* **2018,** *3*, 18008.
(12) Du, N.; Yang, Z.; Liu, X. Y.; Li, Y.; Xu, H. Y. Structural Origin of the Strain-Hardening of Spider Silk. *Adv Funct Mater* **2011,** *21*, 772-778.
(13) Omenetto, F. G.; Kaplan, D. L. New opportunities for an ancient material. *Science* **2010,** *329*, 528-531.
(14) Koh, L.-D.; Cheng, Y.; Teng, C.-P.; Khin, Y.-W.; Loh, X.-J.; Tee, S.-Y.; Low, M.; Ye, E.; Yu, H.-D.; Zhang, Y.-W.; Han, M.-Y. Structures, mechanical properties and applications of silk fibroin materials. *Prog Polym Sci* **2015,** *46*, 86-110.
(15) Fang, G.; Huang, Y.; Tang, Y.; Qi, Z.; Yao, J.; Shao, Z.; Chen, X. Insights into silk formation process: correlation of mechanical properties and structural evolution during artificial spinning of silk fibers. *ACS Biomaterials Science & Engineering* **2016,** *2*, 1992-2000.
(16) Xia, X.-X.; Qian, Z.-G.; Ki, C. S.; Park, Y. H.; Kaplan, D. L.; Lee, S. Y. Native-sized recombinant spider silk protein produced in metabolically engineered Escherichia coli results in a strong fiber. *Proceedings of the National Academy of Sciences* **2010,** *107*, 14059-14063.
(17) Copeland, C. G.; Bell, B. E.; Christensen, C. D.; Lewis, R. V. Development of a process for the spinning of synthetic spider silk. *ACS biomaterials science & engineering* **2015,** *1*, 577-584.
(18) Keten, S.; Xu, Z.; Ihle, B.; Buehler, M. J. Nanoconfinement controls stiffness, strength and mechanical toughness of β-sheet crystals in silk. *Nat Mater* **2010,** *9*, 359-367.
(19) Jin, H.-J.; Kaplan, D. L. Mechanism of silk processing in insects and spiders. *Nature* **2003,** *424*, 1057-1061.
(20) Miller, L. D.; Putthanarat, S.; Eby, R.; Adams, W. Investigation of the nanofibrillar morphology in silk fibers by small angle X-ray scattering and atomic force microscopy. *Int J Biol Macromol* **1999,** *24*, 159-165.

(21) Xu, G.; Gong, L.; Yang, Z.; Liu, X. Y. What makes spider silk fibers so strong? From molecular-crystallite network to hierarchical network structures. *Soft Matter* **2014,** *10*, 2116-23.
(22) Putthanarat, S.; Stribeck, N.; Fossey, S.; Eby, R.; Adams, W. Investigation of the nanofibrils of silk fibers. *Polymer* **2000,** *41*, 7735-7747.
(23) Asakura, T.; Okushita, K.; Williamson, M. P. Analysis of the Structure ofBombyx moriSilk Fibroin by NMR. *Macromolecules* **2015,** *48*, 2345-2357.
(24) Holland, G. P.; Lewis, R. V.; Yarger, J. L. WISE NMR characterization of nanoscale heterogeneity and mobility in supercontracted Nephila clavipes spider dragline silk. *J Am Chem Soc* **2004,** *126*, 5867-5872.
(25) Termonia, Y. Molecular modeling of spider silk elasticity. *Macromolecules* **1994,** *27*, 7378-7381.
(26) Porter, D.; Vollrath, F.; Shao, Z. Predicting the mechanical properties of spider silk as a model nanostructured polymer. *Eur Phys J E Soft Matter* **2005,** *16*, 199-206.
(27) Vollrath, F.; Porter, D. Spider silk as a model biomaterial. *Applied Physics A* **2006,** *82*, 205-212.
(28) Krasnov, I.; Diddens, I.; Hauptmann, N.; Helms, G.; Ogurreck, M.; Seydel, T.; Funari, S. S.; Muller, M. Mechanical properties of silk: interplay of deformation on macroscopic and molecular length scales. *Phys Rev Lett* **2008,** *100*, 048104.
(29) Von Fraunhofer, J.; Sichina, W. Characterization of surgical suture materials using dynamic mechanical analysis. *Biomaterials* **1992,** *13*, 715-720.
(30) Rousseau, M.-E.; Lefèvre, T.; Beaulieu, L.; Asakura, T.; Pézolet, M. Study of protein conformation and orientation in silkworm and spider silk fibers using Raman microspectroscopy. *Biomacromolecules* **2004,** *5*, 2247-2257.
(31) Giesa, T.; Arslan, M.; Pugno, N. M.; Buehler, M. J. Nanoconfinement of spider silk fibrils begets superior strength, extensibility, and toughness. *Nano Lett* **2011,** *11*, 5038-5046.
(32) Yang, Y.; Chen, X.; Shao, Z.; Zhou, P.; Porter, D.; Knight, D. P.; Vollrath, F. Toughness of spider silk at high and low temperatures. *Advanced Materials* **2005,** *17* , 84-88.
(33) Rockwood, D. N.; Preda, R. C.; Yucel, T.; Wang, X.; Lovett, M. L.; Kaplan, D. L. Materials fabrication from Bombyx mori silk fibroin. *Nat Protoc* **2011,** *6* , 1612-31.
(34) Vepari, C.; Kaplan, D. L. Silk as a Biomaterial. *Prog Polym Sci* **2007,** *32*, 991-1007,.
(35) Wang, Q.; Jian, M.; Wang, C.; Zhang, Y. Carbonized Silk Nanofiber Membrane for Transparent and Sensitive Electronic Skin. *Adv Funct Mater* **2017,** *27*, 1605657.
(36) Boekhoven, J.; Brizard, A. M.; van Rijn, P.; Stuart, M. C.; Eelkema, R.; van Esch, J. H. Programmed morphological transitions of multisegment assemblies by molecular chaperone analogues. *Angew Chem Int Ed Engl* **2011,** *50*, 12285-9.
(37) Ling, S.; Qin, Z.; Li, C.; Huang, W.; Kaplan, D. L.; Buehler, M. J. Polymorphic regenerated silk fibers assembled through bioinspired spinning. *Nat Commun* **2017,** *8*, 1387.
(38) Ling, S.; Li, C.; Adamcik, J.; Shao, Z.; Chen, X.; Mezzenga, R. Modulating materials by orthogonally oriented beta-strands: composites of amyloid and silk fibroin fibrils. *Adv Mater* **2014,** *26*, 4569-74.
(39) Loll, B.; Kern, J.; Saenger, W.; Zouni, A.; Biesiadka, J. Towards complete cofactor arrangement in the 3.0 Å resolution structure of photosystem II. *Nature* **2005,** *438*, 1040.
(40) Liu, R.; Deng, Q.; Yang, Z.; Yang, D.; Han, M.-Y.; Liu, X. Y. "Nano-Fishnet" Structure Making Silk Fibers Tougher. *Adv Funct Mater* **2016,** *26*, 5534-5541.
(41) Asakura, T.; Kuzuhara, A.; Tabeta, R.; Saito, H. Conformational characterization of Bombyx mori silk fibroin in the solid state by high-frequency carbon-13 cross polarization-magic angle

spinning NMR, x-ray diffraction, and infrared spectroscopy. *Macromolecules* **1985,** *18*, 1841-1845.

(42) Van Beek, J.; Beaulieu, L.; Schäfer, H.; Demura, M.; Asakura, T.; Meier, B. Solid-state NMR determination of the secondary structure of Samia cynthia ricini silk. *Nature* **2000,** *405*, 1077.

(43) Ling, S.; Li, C.; Adamcik, J.; Wang, S.; Shao, Z.; Chen, X.; Mezzenga, R. Directed Growth of Silk Nanofibrils on Graphene and Their Hybrid Nanocomposites. *ACS Macro Lett* **2014,** *3*, 146-152.

(44) Allen, M. J.; Hud, N. V.; Balooch, M.; Tench, R. J.; Siekhaus, W. J.; Balhorn, R. Tip-radius-induced artifacts in AFM images of protamine-complexed DNA fibers. *Ultramicroscopy* **1992,** *42*, 1095-1100.

(45) Blasi, L.; Longo, L.; Vasapollo, G.; Cingolani, R.; Rinaldi, R.; Rizzello, T.; Acierno, R.; Maffia, M. Characterization of glutamate dehydrogenase immobilization on silica surface by atomic force microscopy and kinetic analyses. *Enzyme Microb Tech* **2005,** *36*, 818-823.

(46) Gosline, J.; Guerette, P.; Ortlepp, C.; Savage, K. The mechanical design of spider silks: from fibroin sequence to mechanical function. *J Exp Biol* **1999,** *202*, 3295-3303.

(47) Hakimi, O.; Knight, D. P.; Vollrath, F.; Vadgama, P. Spider and mulberry silkworm silks as compatible biomaterials. *Composites Part B: Engineering* **2007,** *38*, 324-337.

(48) Calzado-Martin, A.; Encinar, M.; Tamayo, J.; Calleja, M.; San Paulo, A. Effect of Actin Organization on the Stiffness of Living Breast Cancer Cells Revealed by Peak-Force Modulation Atomic Force Microscopy. *ACS Nano* **2016,** *10*, 3365-74.

(49) Zhao, F.; Huang, Y.; Liu, L.; Bai, Y.; Xu, L. Formation of a carbon fiber/polyhedral oligomeric silsesquioxane/carbon nanotube hybrid reinforcement and its effect on the interfacial properties of carbon fiber/epoxy composites. *Carbon* **2011,** *49*, 2624-2632.

(50) Cranford, S. W. Increasing silk fibre strength through heterogeneity of bundled fibrils. *J R Soc Interface* **2013,** *10*, 20130148.

(51) Porter, D.; Vollrath, F. Silk as a Biomimetic Ideal for Structural Polymers. *Adv Mater* **2009,** *21*, 487-492.

(52) Ling, S.; Li, C.; Jin, K.; Kaplan, D. L.; Buehler, M. J. Liquid Exfoliated Natural Silk Nanofibrils: Applications in Optical and Electrical Devices. *Adv Mater* **2016,** *28*, 7783-90.

(53) Ling, S.; Jin, K.; Kaplan, D. L.; Buehler, M. J. Ultrathin Free-Standing Bombyx mori Silk Nanofibril Membranes. *Nano Lett* **2016,** *16*, 3795-800.

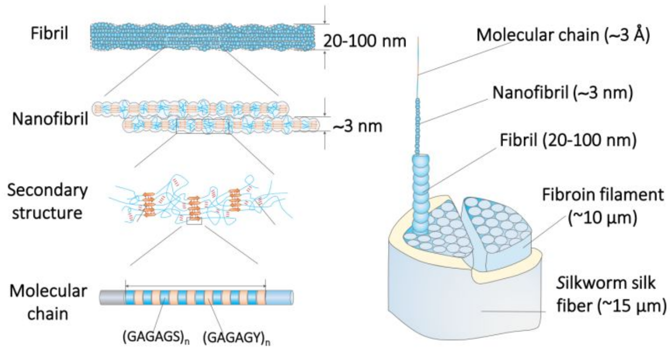
Fibril
20-100 nm
Nanofibril
~3 nm
Secondary structure
Molecular chain
(GAGAGS)$_n$
(GAGAGY)$_n$
Molecular chain (~3 Å)
Nanofibril (~3 nm)
Fibril (20-100 nm)
Fibroin filament (~10 µm)
Silkworm silk fiber (~15 µm)

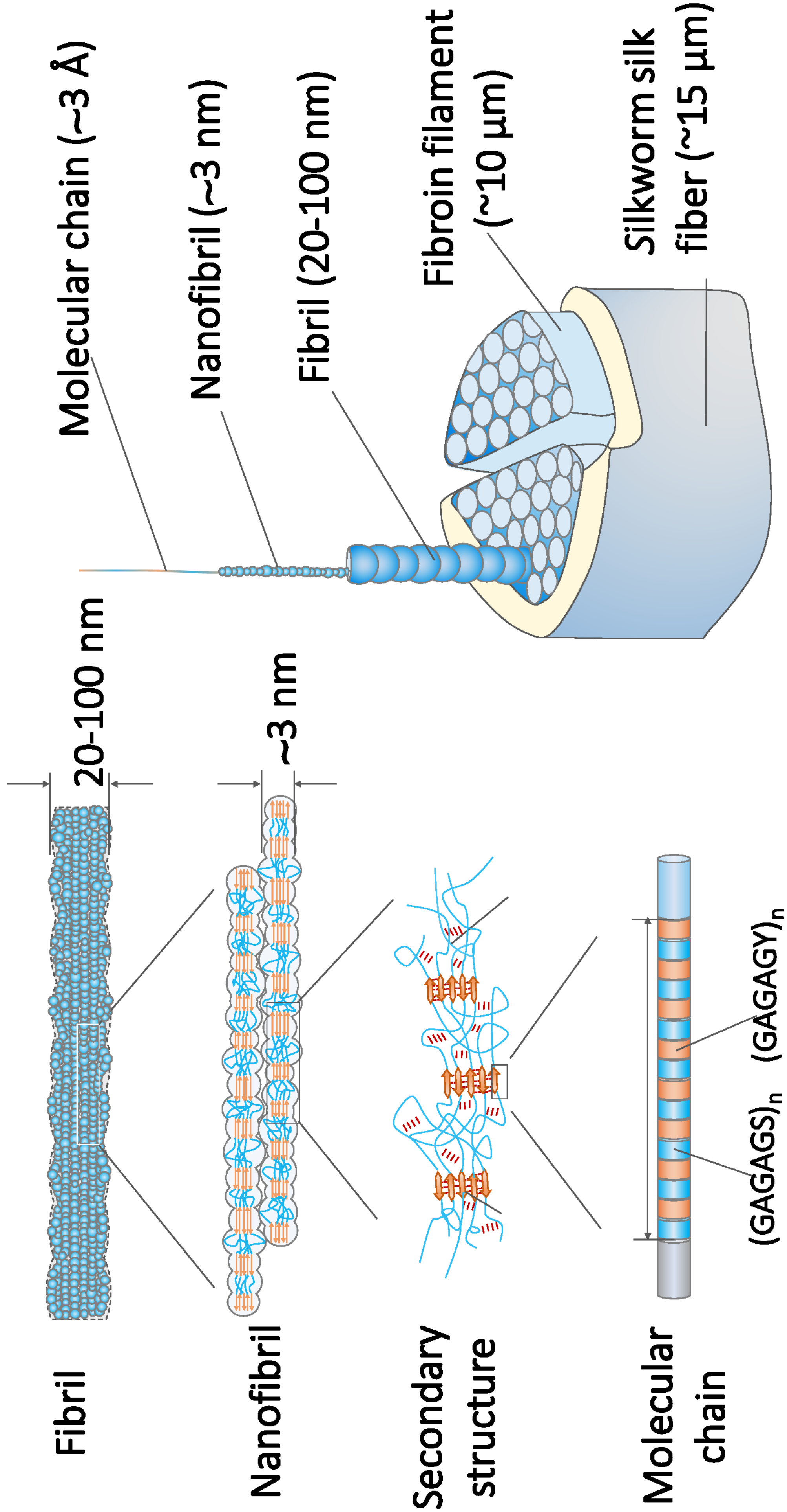
Molecular chain (~3 Å)
Nanofibril (~3 nm)
Fibril (20-100 nm)
Fibroin filament (~10 µm)
Silkworm silk fiber (~15 µm)
20-100 nm
~3 nm
Fibril
Nanofibril
Secondary structure
Molecular chain
$(GAGAGS)_n$
$(GAGAGY)_n$